

Sign problem in Z_3 -symmetric effective Polyakov-line model

Takehiro Hirakida,^{1,*} Junpei Sugano,^{1,†} Hiroaki Kouno,^{2,‡} Junichi Takahashi,^{3,§} and Masanobu Yahiro^{1,¶}

¹*Department of Physics, Graduate School of Sciences, Kyushu University, Fukuoka 819-0395, Japan*

²*Department of Physics, Saga University, Saga 840-8502, Japan*

³*Division of Observation, Fukuoka Aviation Weather Station, Japan Meteorological Agency, Fukuoka 812-0005, Japan*

(Dated: March 6, 2018)

As an effective model corresponding to Z_3 -symmetric QCD (Z_3 -QCD), we construct a Z_3 -symmetric effective Polyakov-line model (Z_3 -EPLM) by using the logarithmic fermion effective action. Since Z_3 -QCD tends to QCD in the zero-temperature limit, Z_3 -EPLM also agrees with the ordinary effective Polyakov-line model (EPLM) there; note that (ordinary) EPLM does not possess Z_3 symmetry. Our main purpose is to discuss a sign problem appearing in Z_3 -EPLM. The action of Z_3 -EPLM is real, when the Polyakov line is not only real but also its Z_3 images. This suggests that the sign problem becomes milder in Z_3 -EPLM than in EPLM. In order to confirm this suggestion, we do lattice simulations for both EPLM and Z_3 -EPLM by using the reweighting method with the phase quenched approximation. In the low-temperature region, the sign problem is milder in Z_3 -EPLM than in EPLM. We also propose a new reweighting method. This makes the sign problem very weak in Z_3 -EPLM.

PACS numbers: 05.50.+q, 12.38.Aw, 25.75.Nq

I. INTRODUCTION

Exploration of the QCD phase diagram at finite temperature T and quark-number chemical potential μ is one of the most challenging subjects in particle and nuclear physics, as well as in cosmology and astrophysics. For $\mu = 0$, lattice QCD (LQCD) simulations as a first-principle calculation are well established and yield much knowledge on hot-QCD matter. For finite μ , however, there is well-known difficulty in LQCD; namely, the so-called sign problem. At finite μ , effective action S_{eff} , which is obtained after the integration of the quark fields in the grand canonical partition function, is complex in general, and we cannot regard $e^{-S_{\text{eff}}}$ as the probability function that determines the realization probability of gauge configurations. This makes the importance sampling method impractical. To evade the sign problem, several approaches, e.g., the reweighting method [1], the Taylor expansion method [2, 3] and the analytic continuation from imaginary μ to real μ [4–9] were used. Recently, great progresses were made by the complex Langevin simulation [10–15] and the Picard-Lefschetz thimble theory [16–19]. However, particularly for the region of $\mu/T > 1$ in μ - T plane, our understanding of the QCD phase diagram is still far from perfection.

It is expected that Z_3 symmetry plays an important role in solving the sign problem. It was conjectured [20] that the center-dressed quark undergoes a new phase with the Fermi-Einstein condensation in cold and dense matter, and the phenomenon is a key to the solution of the Silver Blaze problem [21, 22]. It was shown that, by using the properties of

Z_3 group, an effective center field theory with the sign problem can be transformed into a flux model with no sign problem [23, 24]. In Ref. [25], it was suggested that the sign problem in full QCD with no exact symmetry may be cured to some extent by using Z_3 -averaged subset method. However, these methods are not adequate to solve the sign problem in QCD completely.

In the pure $SU(3)$ gauge theory, Z_3 symmetry is exact and governs the confinement-deconfinement transition. The Polyakov-line (loop) [26] is defined as an exact order parameter of the confinement-deconfinement transition. However, in full QCD with dynamical quarks, Z_3 symmetry is not exact anymore, and it is not trivial that the Polyakov line is an order parameter for the confinement-deconfinement transition [27]. In order to study the relation between the confinement-deconfinement transition and the Polyakov line, Z_3 -symmetric QCD-like theory was proposed in Refs. [28–32]. We call the theory Z_3 -QCD in this paper. Z_3 -QCD was studied at first by the effective model [28–32], and QCD simulations were recently made for $\mu = 0$ [33].

It was conjectured [32] that the sign problem is milder in Z_3 -QCD than in the ordinary QCD. The study of the sign problem in Z_3 -QCD is important, since Z_3 -QCD tends to three-flavor QCD in the limit $T \rightarrow 0$. To examine the conjecture, Hirakida *et al.* [34] constructed a Z_3 -symmetric 3D Potts model as a toy model of Z_3 -QCD, and studied a sign problem appearing in the model. It was found that the sign problem in the Z_3 -symmetric 3D Potts model is much milder than in the ordinary 3D 3-state Potts model [35–37] with no Z_3 symmetry, even when several states are included in the calculations together with three Z_3 -elements. However, the correspondence between Z_3 -QCD and the Z_3 -symmetric 3D Potts model defined in Ref. [34] is only qualitative.

In this paper, we construct a Z_3 -symmetric effective Polyakov-line model (Z_3 -EPLM). The Z_3 -EPLM is an effective model for Z_3 -QCD in the heavy-quark and high-density limit, and is closer to Z_3 -QCD than the Z_3 -symmetric 3D

*hirakida@email.phys.kyushu-u.ac.jp

†sugano@phys.kyushu-u.ac.jp

‡kounoh@cc.saga-u.ac.jp

§j.t.mhjjk.f.c@gmail.com

¶yahiro@phys.kyushu-u.ac.jp

Potts model. First, we show that the fermionic part of Z_3 -EPLM action can be expressed by ‘‘cubic Polyakov line’’ that is invariant under the Z_3 transformation. Second, we find that the confinement state and the three deconfinement states based on Z_3 symmetry are degenerate in Z_3 -EPLM, when the pure-gauge contribution is neglected in the path integral. Doing lattice calculations based on the reweighting method with the phase quenched approximation, we conclude that, at low temperature, the sign problem is milder in Z_3 -EPLM than in EPLM with no Z_3 symmetry. Finally, we propose a new reweighting method. This method reduces the sign problem considerably. In particular, the problem becomes very weak in Z_3 -EPLM.

This paper is organized as follows. In Sec. II, we review the formalism of Z_3 -QCD. In Sec. III, we formulate Z_3 -EPLM, and also discuss how important the particle-hole (P-H) symmetry [38] is in EPLM. In Sec. IV, the reweighting methods we use are explained. Numerical simulations are done for the models in Sec. V. Section VI is devoted to a summary.

II. Z_3 -QCD

In this section, we review the formalism of Z_3 -QCD [28–34]. The grand canonical partition function of three-flavor QCD with a common quark mass m , quark-number chemical potential μ and temperature T ($= 1/\beta$) is given by

$$Z = \int \mathcal{D}A_\mu \mathcal{D}\bar{q} \mathcal{D}q e^{-S}; \quad (1)$$

$$S = S_G + S_Q \\ = \int_0^\beta dx_4 \int_{-\infty}^\infty d^3\mathbf{x} \mathcal{L}_G + \int_0^\beta dx_4 \int_{-\infty}^\infty d^3\mathbf{x} \mathcal{L}_Q; \quad (2)$$

$$\mathcal{L}_G = \frac{1}{4g^2} F_{\mu\nu}^a{}^2 = \frac{1}{2g^2} \text{Tr} [F_{\mu\nu}^2], \quad (3)$$

$$\mathcal{L}_F = \bar{q} \mathcal{M} q, \quad (4)$$

where

$$\mathcal{M} = \gamma_\mu D_\mu + m - \mu \gamma_4, \quad (5)$$

$$F_{\mu\nu} = \partial_\mu A_\nu - \partial_\nu A_\mu + i[A_\mu, A_\nu], \quad (6)$$

$$D_\mu = \partial_\mu - iA_\mu, \quad A_\mu = g \sum_{a=1}^8 A_\mu^a \frac{\lambda^a}{2}, \quad (7)$$

with the quark field q , the gluon field A_μ^a , the gauge coupling g and the Gell-Mann matrices λ^a . The temporal anti-periodic boundary condition on the quark field is given by

$$q(x_4 = \beta, \mathbf{x}) = -q(x_4 = 0, \mathbf{x}), \quad (8)$$

while the gluon field A_μ^a obeys the periodic boundary condition in the temporal direction. Note that q is a vector also in flavor space. Hereafter, we denote each flavor component of q as q_f .

The Lagrangian density $\mathcal{L}_G + \mathcal{L}_F$ is invariant under the Z_3 transformation,

$$q \rightarrow q' = Uq, \quad A_\mu \rightarrow A'_\mu = UA_\mu U^{-1} + i(\partial_\mu U)U^{-1}, \quad (9)$$

where $U = \exp(i\alpha_a(x_4, \mathbf{x})\lambda^a/2)$ is an element of $SU(3)$ group characterized by real functions $\alpha_a(x_4, \mathbf{x})$ satisfying the temporal boundary condition

$$U(x_4 = \beta, \mathbf{x}) = e^{-i2\pi k/3} U(x_4 = 0, \mathbf{x}) \quad (10)$$

for any integer k . However, the condition (8) on the quark field is changed by the Z_3 transformation (9) into

$$q(x_4 = \beta, \mathbf{x}) = -e^{i2\pi k/3} q(x_4 = 0, \mathbf{x}). \quad (11)$$

Thus, in full QCD with dynamical quarks, Z_3 symmetry is explicitly broken through the quark boundary condition.

To recover Z_3 symmetry, one can consider the flavor dependent twist boundary condition (FTBC) [28–32],

$$q_f(x_4 = \beta, \mathbf{x}) = -e^{-i\theta_f} q_f(x_4 = 0, \mathbf{x}); \\ \theta_f = \frac{2\pi}{3} f \quad (f = -1, 0, 1), \quad (12)$$

instead of the condition (8). Here, the flavor indices are represented by the number $-1, 0, 1$ for convenience. Under the Z_3 transformation (9), the FTBC (12) is transformed into

$$q_f(x_4 = \beta, \mathbf{x}) = -e^{-i\theta'_f} q_f(x_4 = 0, \mathbf{x}); \\ \theta'_f = \frac{2\pi}{3} (f - k) \quad (f = -1, 0, 1). \quad (13)$$

The transformed boundary condition (13) returns to the original one (12) by relabeling the flavor indices $f - k$ as f . Hence, the QCD-like theory with the FTBC (12) is invariant under the Z_3 transformation. In this paper, this theory is referred to as Z_3 -QCD. It should be noted that Z_3 -QCD agrees with original QCD in the limit $T \rightarrow 0$, since the boundary condition is not relevant in this limit.

When the quark fields q_f are transformed into [39]

$$q_f \rightarrow e^{-i\theta_f T x_4} q_f, \quad (14)$$

the FTBC (12) returns to the ordinary anti-periodic boundary condition (8). However, the quark part \mathcal{L}_F of the Lagrangian density is changed into

$$\mathcal{L}_F^{\hat{\theta}} = \bar{q}(\gamma_\mu D_\mu + m - i\hat{\theta}T\gamma_4)q, \quad (15)$$

where

$$\hat{\theta} = \text{diag}(\theta_{-1}, \theta_0, \theta_1) = \text{diag}(-2\pi/3, 0, 2\pi/3) \quad (16)$$

is the flavor-dependent imaginary chemical potential normalized by T . (In the pioneering work of Ref. [40], Hasenfratz and Toussaint introduced the fictitious flavor-dependent imaginary chemical potential to make the non-zero triality sectors of canonical partition function vanish more rigidly in LQCD simulations.) The flavor-dependent imaginary chemical potential partially breaks flavor $SU(3)$ symmetry. In the chiral limit $m \rightarrow 0$, due to the existence of $\hat{\theta}$, global $SU_V(3) \otimes SU_A(3)$ symmetry is broken to $(U_V(1))^2 \otimes (U_A(1))^2$ [30]. The remaining symmetry is broken into $(U_V(1))^2$, if chiral symmetry is spontaneously broken. Recently, the FTBC was also discussed in the context of spontaneous chiral symmetry breaking [41, 42].

III. Z_3 -SYMMETRIC EFFECTIVE POLYAKOV-LINE MODEL

A. Effective Polyakov-line model

In this section, we formulate Z_3 -symmetric EPLM and examine its properties. Before going to the discussion, we first review the ordinary EPLM. The grand canonical partition function of EPLM is given by [11, 15]

$$Z = \int \mathcal{D}U \exp(-S_F - S_G); \quad (17)$$

$$S_F = \sum_{\mathbf{x}} L_F(\mathbf{x}), \quad (18)$$

$$S_G = -\kappa \sum_{\mathbf{x}} \sum_{i=1}^3 \left(\text{Tr}[U_{\mathbf{x}}] \text{Tr}[U_{\mathbf{x}+\mathbf{i}}^\dagger] + \text{Tr}[U_{\mathbf{x}}^\dagger] \text{Tr}[U_{\mathbf{x}+\mathbf{i}}] \right), \quad (19)$$

where $U_{\mathbf{x}}$ is the Polyakov-line (loop) holonomy and the symbol \mathbf{i} is a unit vector for i -th direction. The site variable \mathbf{x} runs over a 3-dimensional lattice.

The constant parameter κ is related to temperature $T = 1/\beta$. Roughly speaking, large (small) κ corresponds to high (low) temperature [35], but the relation is not so simple. In this paper, we treat κ just as a parameter independent of T , while the other parameters with the energy dimension are always normalized by T . In Ref. [15], a more-complicated form with a lot of parameters is used for the gauge action S_G , but we take a simple form as in Ref. [11] in order to know qualitative properties of the phase structure and the sign problem of this model in a wide range of the parameter set. Using the temporal gauge, we parameterize $U_{\mathbf{x}}$ as [15]

$$U_{\mathbf{x}} = \text{diag}(e^{i\varphi_{r,\mathbf{x}}}, e^{i\varphi_{g,\mathbf{x}}}, e^{i\varphi_{b,\mathbf{x}}}), \quad (20)$$

$$U_{\mathbf{x}}^\dagger = \text{diag}(e^{-i\varphi_{r,\mathbf{x}}}, e^{-i\varphi_{g,\mathbf{x}}}, e^{-i\varphi_{b,\mathbf{x}}}) \quad (21)$$

with the condition $\varphi_{r,\mathbf{x}} + \varphi_{g,\mathbf{x}} + \varphi_{b,\mathbf{x}} = 0$, and define the (traced) Polyakov line (loop) $P_{\mathbf{x}}$ and its conjugate $P_{\mathbf{x}}^*$ as

$$P_{\mathbf{x}} = \frac{1}{3} \text{Tr}[U_{\mathbf{x}}] = \frac{1}{3} (e^{i\varphi_{r,\mathbf{x}}} + e^{i\varphi_{g,\mathbf{x}}} + e^{i\varphi_{b,\mathbf{x}}}), \quad (22)$$

$$P_{\mathbf{x}}^* = \frac{1}{3} \text{Tr}[U_{\mathbf{x}}^\dagger] = \frac{1}{3} (e^{-i\varphi_{r,\mathbf{x}}} + e^{-i\varphi_{g,\mathbf{x}}} + e^{-i\varphi_{b,\mathbf{x}}}). \quad (23)$$

In this paper, instead of $U_{\mathbf{x}}$ and $U_{\mathbf{x}}^\dagger$, we treat the phase variables $\varphi_{r,\mathbf{x}}$ and $\varphi_{g,\mathbf{x}}$ as dynamical variables. The Haar measure $\mathcal{D}U$ in the path integral (17) is rewritten into [15]

$$\mathcal{D}U = e^{-S_H(\varphi_{r,\mathbf{x}}, \varphi_{g,\mathbf{x}})} \mathcal{D}\varphi_{r,\mathbf{x}} \mathcal{D}\varphi_{g,\mathbf{x}}; \quad (24)$$

$$S_H = \sum_{\mathbf{x}} L_H(\mathbf{x}), \quad (25)$$

$$L_H(\mathbf{x}) = -\log \left\{ \sin^2 \left(\frac{\varphi_{r,\mathbf{x}} - \varphi_{g,\mathbf{x}}}{2} \right) \times \sin^2 \left(\frac{2\varphi_{r,\mathbf{x}} + \varphi_{g,\mathbf{x}}}{2} \right) \sin^2 \left(\frac{\varphi_{r,\mathbf{x}} + 2\varphi_{g,\mathbf{x}}}{2} \right) \right\}. \quad (26)$$

Note that, for simplicity of notation, we use dimensionless volume $V = N_s^3$ and dimensionless Lagrangian density L , where N_s is the number of lattice sites in one spatial direction. Hereafter, for simplicity, we refer to this three-flavor EPLM with no Z_3 symmetry as EPLMWO.

For the fermionic Lagrangian density, we consider a logarithmic one of Ref. [15]:

$$\begin{aligned} L_F[\mu, \varphi_{c,\mathbf{x}}] &= -\log \left(\det \left[1 + e^{\beta(\mu-M)} U_{\mathbf{x}} \right]^{2N_f} \right. \\ &\quad \times \det \left[1 + e^{-\beta(\mu+M)} U_{\mathbf{x}}^\dagger \right]^{2N_f} \left. \right) \\ &= -2N_f \sum_{c=r,g,b} \left\{ \log \left(1 + e^{\beta(\mu-M+i\varphi_{c,\mathbf{x}})} \right) \right. \\ &\quad \left. + \log \left(1 + e^{-\beta(\mu+M+i\varphi_{c,\mathbf{x}})} \right) \right\} \\ &= -2N_f \left\{ \log \left(1 + 3e^{\beta(\mu-M)} P_{\mathbf{x}} \right) \right. \\ &\quad \left. + 3e^{2\beta(\mu-M)} P_{\mathbf{x}}^* + e^{3\beta(\mu-M)} \right) \\ &\quad \left. + \log \left(1 + 3e^{-\beta(\mu+M)} P_{\mathbf{x}}^* \right) \right. \\ &\quad \left. + 3e^{-2\beta(\mu+M)} P_{\mathbf{x}} + e^{-3\beta(\mu+M)} \right\}, \quad (27) \end{aligned}$$

where M is the quark mass.

It is easily seen that, in the limit $M \rightarrow \infty$, L_F becomes real at $\mu = M$, since $e^{\beta(\mu-M)} = e^{2\beta(\mu-M)} = 1$ and $e^{-\beta(\mu+M)} = e^{-2\beta(\mu+M)} = 0$ in the last line of Eq. (27). As seen below, the reality of L_F at $\mu = M$ is related to the particle-hole symmetry in EPLM.

B. Particle-hole symmetry

The particle contribution in L_F can be rewritten into

$$\begin{aligned} L_{F,p}[\mu = M - \Delta\mu, \varphi_{c,\mathbf{x}}] &= -2N_f \sum_{c=r,g,b} \log \left(1 + e^{\beta(-\Delta\mu+i\varphi_{c,\mathbf{x}})} \right) \\ &= -2N_f \sum_{c=r,g,b} \left\{ \beta(-\Delta\mu + i\varphi_{c,\mathbf{x}}) \right. \\ &\quad \left. + \log \left(1 + e^{\beta(\Delta\mu-i\varphi_{c,\mathbf{x}})} \right) \right\} \\ &= 6N_f \beta \Delta\mu - 2N_f \sum_{c=r,g,b} \log \left(1 + e^{\beta(\Delta\mu-i\varphi_{c,\mathbf{x}})} \right) \\ &= 6N_f \beta \Delta\mu + L_{F,p}[\mu = M + \Delta\mu, -\varphi_{c,\mathbf{x}}]. \quad (28) \end{aligned}$$

The term $6N_f \beta \Delta\mu$ in the last line of (28) does not depend on the dynamical variable $\varphi_{c,\mathbf{x}}$ and does not contribute to the expectation value of physical quantities. Hence, the relation $L_{F,p}[\mu = M - \Delta\mu, \varphi_{c,\mathbf{x}}] = L_{F,p}[\mu = M + \Delta\mu, -\varphi_{c,\mathbf{x}}]$ is effectively satisfied. Furthermore, since the antiparticle contribution in L_F is negligible in the limit $M \rightarrow \infty$, we obtain $\langle \bar{P}(\mu = M - \Delta\mu) \rangle = \langle \bar{P}^*(\mu = M + \Delta\mu) \rangle$ and $\langle \bar{P}^*(\mu = M - \Delta\mu) \rangle = \langle \bar{P}(\mu = M + \Delta\mu) \rangle$. We have a relation $\langle O(\mu = M - \Delta\mu) \rangle = \langle O(\mu = M + \Delta\mu) \rangle$ for any quantity

O that does not depend on the sign of $\varphi_{c,\mathbf{x}}$ and has no explicit μ dependence. This relation is nothing but the particle-hole (P-H) symmetry [38]. From this symmetry, one can easily derive the relation $L_F[\mu = M, \varphi_{c,\mathbf{x}}] = L_{F,P}[\mu = M, -\varphi_{c,\mathbf{x}}]$ in the limit $M \rightarrow \infty$. This relation ensures that L_F is real at $\mu = M$.

It should be remarked that the effects of spatial momenta of quarks make the P-H symmetry invisible. In fact, in the Polyakov-loop extended Nambu–Jona-Lasinio (PNJL) model [43–47], the quark-loop contribution $\Omega_{\text{PNJL},F}$ of the thermodynamical potential density is given, under the mean field approximation, as

$$\begin{aligned} \Omega_{\text{PNJL},F} = & -2N_f \sum_{c=r,g,b} \int \frac{dp}{2\pi^2} \left\{ E_p \right. \\ & + T \log \left(1 + e^{\beta(\mu - E_p)} e^{i\phi_c} \right) \\ & \left. + T \log \left(1 + e^{-\beta(\mu + E_p)} e^{-i\phi_c} \right) \right\}, \end{aligned} \quad (29)$$

where $E_p = \sqrt{p^2 + M^2}$, p is the absolute value of quark spatial momentum, and ϕ_c is similar to $\varphi_{c,\mathbf{x}}$ but does not depend on the spatial coordinate \mathbf{x} . Up to the factor $\mu - E_p$ that does not depend on ϕ_c , the logarithmic function $\log(1 + e^{\beta(\mu - E_p)} e^{i\phi_c})$ is symmetric under the transformation, $\mu = E_p - \Delta\mu \rightarrow \mu = E_p + \Delta\mu$ and $\phi_c \rightarrow -\phi_c$, but the location of the symmetric point $\mu = E_p$ depends on p . Hence, the symmetry is invisible when the integration over p is performed. The symmetry does not appear explicitly in QCD where quarks have spatial momenta. Therefore, the appearance of the *explicit* P-H symmetry indicates the limitation of EPLM. The EPLM is considered to be valid as an effective model of QCD only in the region where μ is not much larger than M .

C. Z_3 -symmetric effective Polyakov-line model (Z_3 -EPLM)

Since the traced Polyakov line is not invariant under the Z_3 transformation, the Lagrangian density (27) is not invariant under the Z_3 transformation. To preserve Z_3 symmetry, we consider the three-flavor case and introduce the flavor-dependent imaginary chemical potential $i\theta_f T$ ($f = u, d, s$), where $(\theta_u, \theta_d, \theta_s) = (2\pi/3, -2\pi/3, 0)$. The corresponding Lagrangian density is given by

$$\begin{aligned} L_{F,Z_3}[\mu, \varphi_{c,\mathbf{x}}] \\ = & -2 \sum_{f=u,d,s} \sum_{c=r,g,b} \left\{ \log \left(1 + e^{\beta(\mu - M + i\theta_f + i\varphi_{c,\mathbf{x}})} \right) \right. \\ & \left. + \log \left(1 + e^{-\beta(\mu + M + i\theta_f + i\varphi_{c,\mathbf{x}})} \right) \right\} \end{aligned}$$

$$\begin{aligned} = & -2 \sum_{c=r,g,b} \left\{ \log \left(1 + e^{3\beta(\mu - M + i\varphi_{c,\mathbf{x}})} \right) \right. \\ & \left. + \log \left(1 + e^{-3\beta(\mu + M + i\varphi_{c,\mathbf{x}})} \right) \right\} \\ = & -2 \log \left(1 + 3e^{3\beta(\mu - M)} Q_{\mathbf{x}} \right. \\ & \left. + 3e^{6\beta(\mu - M)} Q_{\mathbf{x}}^* + e^{9\beta(\mu - M)} \right) \\ & -2 \log \left(1 + 3e^{-3\beta(\mu + M)} Q_{\mathbf{x}}^* \right. \\ & \left. + 3e^{-6\beta(\mu + M)} Q_{\mathbf{x}} + e^{-9\beta(\mu + M)} \right), \end{aligned} \quad (30)$$

where “(traced) cubic Polyakov-line” $Q_{\mathbf{x}}$ and its conjugate $Q_{\mathbf{x}}^*$ are defined by

$$Q_{\mathbf{x}} = \frac{1}{3} \text{Tr} [(U_{\mathbf{x}})^3] = \frac{1}{3} (e^{i3\varphi_{r,\mathbf{x}}} + e^{i3\varphi_{g,\mathbf{x}}} + e^{i3\varphi_{b,\mathbf{x}}}), \quad (31)$$

$$Q_{\mathbf{x}}^* = \frac{1}{3} \text{Tr} [(U_{\mathbf{x}}^\dagger)^3] = \frac{1}{3} (e^{-3i\varphi_{r,\mathbf{x}}} + e^{-3i\varphi_{g,\mathbf{x}}} + e^{-3i\varphi_{b,\mathbf{x}}}). \quad (32)$$

It is easy to derive

$$Q_{\mathbf{x}} = 9 \{ (P_{\mathbf{x}})^3 - P_{\mathbf{x}} P_{\mathbf{x}}^* \} + 1, \quad (33)$$

$$Q_{\mathbf{x}}^* = 9 \{ (P_{\mathbf{x}}^*)^3 - P_{\mathbf{x}} P_{\mathbf{x}}^* \} + 1. \quad (34)$$

From (33) and (34), it is clear that, in L_{F,Z_3} , the degeneration between the “deconfinement” gauge state with $P_{\mathbf{x}} = 1$ and the “confinement” state with $P_{\mathbf{x}} = 0$ [30] occurs, since $Q_{\mathbf{x}} = Q_{\mathbf{x}}^* = 1$ in both the states. Note that the cubic Polyakov line is not an order parameter of the confinement-deconfinement transition, since it is invariant under the Z_3 -transformation. This property of $Q_{\mathbf{x}}$ resembles that of the Polyakov line $P_{\mathbf{x}}^{\text{adj}}$ in the adjoint representation [30]. However, there is an essential difference between them. In fact, $P_{\mathbf{x}}^{\text{adj}}$ is related to $P_{\mathbf{x}}$ as

$$P_{\mathbf{x}}^{\text{adj}} = \frac{1}{9} (9P_{\mathbf{x}} P_{\mathbf{x}}^* - 1). \quad (35)$$

Hence, it is Z_3 -invariant and real. However, $Q_{\mathbf{x}}$ is Z_3 -invariant but not real in general. The sign problem exists in Z_3 -EPLM, since $\text{Im}[Q_{\mathbf{x}}]$ can be finite. We also remark that, as in the case of the ordinary EPLM, Z_3 -EPLM has the explicit P-H symmetry that does not appear in Z_3 -QCD itself. Hence Z_3 -EPLM is also valid as an effective model of Z_3 -QCD only in the region where μ is not much larger than M .

D. Fermion potential in EPLM

In this subsection, we examine properties of the fermion potential L_F in EPLM. Note that the Lagrangian density or the potential is dimensionless in our definition.

In Fig. 1, the values of $P_{\mathbf{x}}$ and $Q_{\mathbf{x}}$ are shown in their complex planes. At first glance, $Q_{\mathbf{x}}$ has the same structure as $P_{\mathbf{x}}$ in the complex plane. However, there is an essential difference between them. In the complex plane of $P_{\mathbf{x}}$, points $(-1/2, \pm\sqrt{3}/2)$ are Z_3 -images of a deconfinement

state $P_x = 1 = (1, 0)$. However, in the complex plane of Q_x , points $(-1/2, \pm\sqrt{3}/2)$ are not Z_3 -images of $P_x = 1$. The Z_3 -images of $P_x = 1$ are degenerate with $P_x = 1$ that corresponds to point $(1, 0)$ in the complex plane of Q_x .

Furthermore, as already mentioned in the previous subsection, the confinement state $P_x = 0$ is also degenerate with $P_x = 1$ corresponding to point $(1, 0)$ in the complex plane of Q_x . More generally, the states $P_x = be^{\pm i2\pi/3}$ ($b = -1/3 \sim 1$) are degenerate with $P_x = b$ corresponding to the real axis in the complex plane of Q_x .

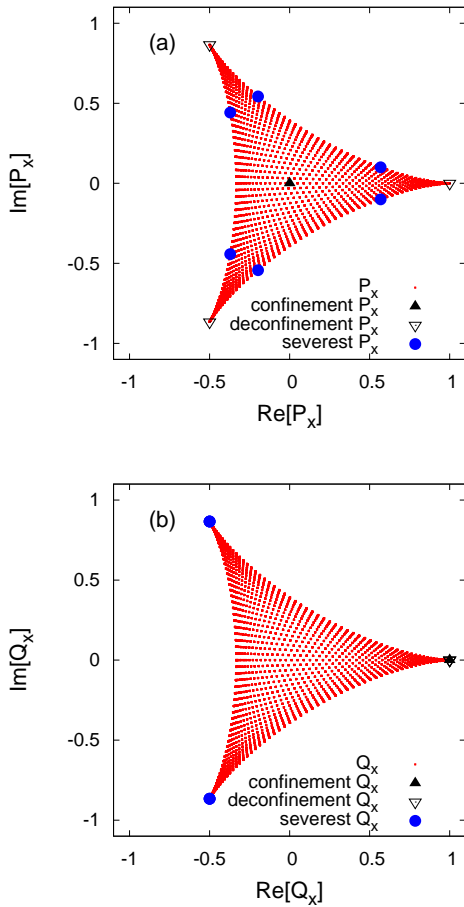


Fig. 1: Allowed regions of (a) P_x and (b) Q_x in the complex plane. In (a), three vertices correspond to the deconfinement points $(1, 0)$, $(-1/2, \sqrt{3}/2)$ and $(-1/2, -\sqrt{3}/2)$, while they are degenerate at the point $(1, 0)$ in (b). In (b), the confinement point is also degenerate with the three deconfinement points. In Z_3 -EPLM, the sign problem is severest at the blue circles.

In the complex Q_x plane, the origin corresponds to a configuration $(\varphi_{r,x}, \varphi_{g,x}, \varphi_{b,x}) = (2\pi/9, -2\pi/9, 0)$ and its Weyl symmetry transformations, and points $(-1/2, \pm\sqrt{3}/2)$ correspond to configurations $(\varphi_{r,x}, \varphi_{g,x}, \varphi_{b,x}) = (\pm 2\pi/9, \pm 2\pi/9, \mp 4\pi/9)$ and their Z_3 and/or Weyl symmetry transformations. The latter points are denoted by the solid circles in Fig. 1. At these points, the absolute value of

$\text{Im}[Q_x]$ becomes maximum and the sign problem is severest in Z_3 -EPLM when these states are favored.

Since P_x can be complex in general, the reality of the action is not ensured at finite μ and a sign problem occurs in EPLM. However, for simplicity, we ignore the effects of imaginary part $\text{Im}[L_F]$ (or $\text{Im}[L_{F,Z_3}]$) in this subsection. If the sign problem is serious, the following discussion may not be applicable. We will discuss the sign problem in EPLM and Z_3 -EPLM in Sec. IV B.

In Fig. 2, the real part $\text{Re}[L_F]$ of EPLMWO is shown in $\varphi_{r,x}-\varphi_{g,x}$ plane. It should be noted that, in addition to points (configurations) shown in Fig. 2, there are the configurations that are obtained from configurations presented in Fig. 2 by performing the Weyl-symmetry transformation. It is seen that $\text{Re}[L_F]$ takes a minimum at the origin where $P_x = 1$. Therefore, probabilistically, the deconfinement state is more favorable than the confinement state if only the fermion potential is considered. Note that Z_3 -images of the origin, namely, points $(\varphi_{r,x}, \varphi_{g,x}) = (2\pi/3, 2\pi/3), (-2\pi/3, -2\pi/3)$ are not favored by the fermion potential, since Z_3 symmetry is explicitly broken.

The qualitative properties of L_F , mentioned above, is independent of μ , but the relative energy-difference ratio $R \equiv (\text{Re}[L_F(\text{max}) - L_F(\text{min})]) / |\text{Re}[L_F(\text{min})]|$ between maximum and minimum values of $\text{Re}[L_F]$ is small when $\mu = M$.

Figure 3 shows $\text{Re}[L_{F,Z_3}]$ of Z_3 -EPLM in $\varphi_{r,x}-\varphi_{g,x}$ plane. There are nine minimum points for each panel. The minimum points $(\varphi_{r,x}, \varphi_{g,x}) = (-2\pi/3, -2\pi/3), (0, 0), (2\pi/3, 2\pi/3)$ correspond to the deconfinement state and the other six points correspond to confinement state. These nine states are degenerate. The relative energy-difference ratio R between maximum and minimum values of $\text{Re}[L_{F,Z_3}]$ is very small when $\mu = M$.

The degeneracy of the confinement and deconfinement states in the fermion effective action has a very important meaning. It means only the pure gauge contribution determines which configuration is probabilistically favorable. Figure 4 shows L_H in $\varphi_{r,x}-\varphi_{g,x}$ plane. It is seen that L_H has a minimum at confinement points. Hence, the confinement state is favored in Z_3 -EPLM with $N_s = 1$, since there is no kinetic term in that case.

In the case of EPLMWO, even in the case of $N_s = 1$, the situation is more complicated. In this case, S_H favors the confinement state, while S_F does the deconfinement one as mentioned above. Which state is favored? It depends on parameters taken in the model. If M is large and μ is smaller than M , the confinement state is favorably realized, since the difference $\Delta L_{F,R} \equiv \text{Re}[L_F(P_x = 0) - L_F(P_x = 1)]$ is suppressed by the large M . Meanwhile, if μ is larger than M , the contribution of $\Delta L_{F,R}$ may be large enough to realize the deconfinement state.

In EPLM with $N_s > 1$, the gluon kinetic term S_G with parameter κ exists. Since S_G favors an ordered deconfinement configuration, the deconfinement phase is realized as an ordered phase when κ is large.

It should be remarked that, when $N_s > 1$, the spatial average value $\bar{P} = \frac{1}{V} \sum_x P_x$ can be zero even if $P_x \neq 0$. In fact,

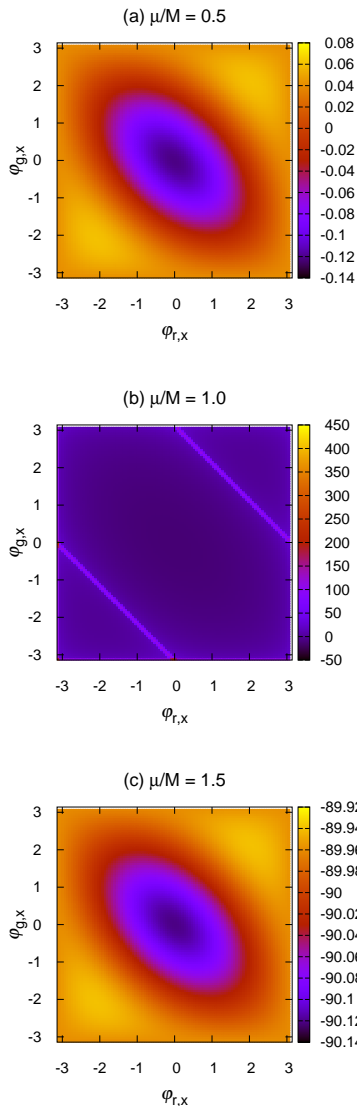


Fig. 2: $\text{Re}[L_F]$ in $\varphi_{r,x}-\varphi_{g,x}$ plane for the case of EPLMWO. The fermion potential takes minimum at the origin. In the calculation, we set $M/T = 10$, and set (a) $\mu = 0.5M$, (b) $\mu = M$, and (c) $\mu = 1.5M$, respectively. Note $\varphi_{b,x} = -\varphi_{r,x} - \varphi_{g,x}$. Due to the P-H symmetry, the result in (c) is (almost) the same as that in (a) up to the total scale factor.

as seen later in Sec. V A, such a cancellation does happen at small κ and μ . In this case, the confinement phase appears as a random phase in which P_x fluctuates largely. Note that, in EPLM, the confinement state $P_x = 0$ and the deconfinement state $P_x = 1$ preserve the reality of the action. Particularly for Z_3 -EPLM, the Z_3 -images of $P_x = 1$ also preserve the reality. However, fluctuations of P_x in the random phase cause the sign problem when μ increases.

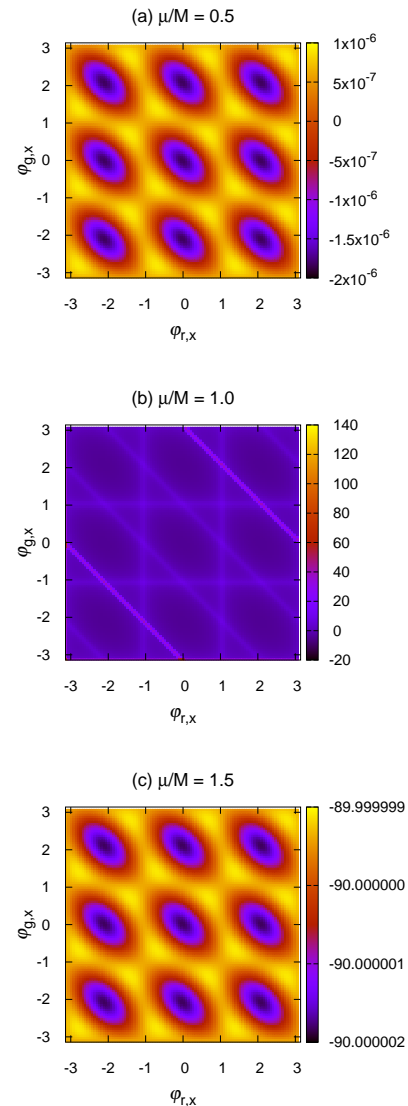


Fig. 3: $\text{Re}[L_F, Z_3]$ in $\varphi_{r,x}-\varphi_{g,x}$ plane for the case of Z_3 -EPLM. The fermion potential Largangian takes minimum at the confinement and deconfinement points. In the calculation, we set $M/T = 10$, and set (a) $\mu = 0.5M$, (b) $\mu = M$, and (c) $\mu = 1.5M$, respectively. Note $\varphi_{b,x} = -\varphi_{r,x} - \varphi_{g,x}$. Due to the P-H symmetry, the result in (c) is (almost) the same as that in (a) up to the total scale factor.

IV. REWEIGHTING METHODS

A. Phase quenched approximation and reweighting method

Since, at finite μ , both EPLMWO and Z_3 -EPLM have the sign problem in its path integral formalism, we use the phase quenched approximation (PQA). Using the approximate probability function F'/Z' , we calculate the approximate average

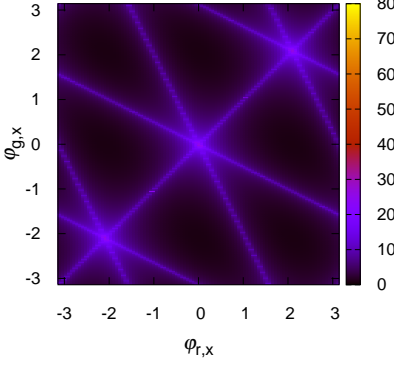


Fig. 4: The effective potential L_H induced from the Haar measure is shown in $\varphi_{r,x}-\varphi_{g,x}$ plane. L_H takes minimum at the confinement points.

value of a physical quantity O as

$$\begin{aligned} \langle O \rangle' &= \frac{\int \mathcal{D}\varphi_r \mathcal{D}\varphi_g O(\varphi_{r,x}, \varphi_{g,x}) F'(\varphi_{r,x}, \varphi_{g,x})}{Z'}; \\ F'(\varphi_{r,x}, \varphi_{g,x}) &= e^{-S_0 - S_{F,R}}, \\ Z' &= \int \mathcal{D}\varphi_r \mathcal{D}\varphi_g F'(\varphi_{r,x}, \varphi_{g,x}), \end{aligned} \quad (36)$$

where $S_0 = S_G + S_H$ and $S_{F,R} = \text{Re}[S_F]$. The phase factor W' is given by

$$\begin{aligned} W' &= \frac{Z}{Z'} = \frac{\int \mathcal{D}\varphi_r \mathcal{D}\varphi_g [e^{-iS_{F,I}}] F'(\varphi_{r,x}, \varphi_{g,x})}{Z'} \\ &= \langle e^{-iS_{F,I}} \rangle' = \left\langle \frac{F}{F'} \right\rangle'; \\ F(\varphi_{r,x}, \varphi_{g,x}) &= e^{-S_0 - S_F} = e^{-S_0 - S_{F,R} - iS_{F,I}}, \\ Z &= \int \mathcal{D}\varphi_r \mathcal{D}\varphi_g F(\varphi_{r,x}, \varphi_{g,x}), \end{aligned} \quad (37)$$

where $S_{F,I} = \text{Im}[S_F]$. Taking the partial average of two configurations $(\varphi_{r,x}, \varphi_{g,x})$ and $(\varphi'_{r,x}, \varphi'_{g,x})$ that satisfy $(\varphi'_{r,x}, \varphi'_{g,x}) = (-\varphi_{r,x}, -\varphi_{g,x})$, we obtain [34]

$$\begin{aligned} W' &= \frac{\int \mathcal{D}\varphi_r \mathcal{D}\varphi_g [\cos(S_{F,I})] F'(\varphi_{r,x}, \varphi_{g,x})}{Z'} \\ &= \langle \cos(S_{F,I}) \rangle', \end{aligned} \quad (38)$$

since $S_{F,I}(\varphi'_{r,x}, \varphi'_{g,x}) = -S_{F,I}(\varphi_{r,x}, \varphi_{g,x})$. Hence the phase factor is real and $|W'| \leq 1$ is satisfied. Using the reweighting method, one can obtain the true expectation value $\langle O \rangle$ as

$$\begin{aligned} \langle O \rangle &= \frac{\int \mathcal{D}\varphi_r \mathcal{D}\varphi_g [O(\varphi_{r,x}, \varphi_{g,x})] F(\varphi_{r,x}, \varphi_{g,x})}{Z} \\ &= \frac{\int \mathcal{D}\varphi_r \mathcal{D}\varphi_g [O e^{-iS_{F,I}}] F'}{Z'} \times \frac{Z'}{Z} \\ &= \frac{\langle O e^{-iS_{F,I}} \rangle'}{W'}. \end{aligned} \quad (39)$$

In this paper, we refer this reweighting method as ‘‘phase quenched reweighting (PQRW)’’.

If $\cos(S_{F,I})$ can have a negative sign, the absolute value of the phase factor (38) becomes small due to the cancellation between the configurations with positive $\cos(S_{F,I})$ and those with negative $\cos(S_{F,I})$. In actual simulations, the smallness of the absolute value of W' causes large errors in the division (39) and makes the calculation results unreliable. Hence, in PQRW, the phase factor W' indicates how serious the sign problem is.

B. Sign problem in EPLM

In order to see the fact that the sign problem is milder in Z_3 -EPLM than in EPLMWO, we examine the imaginary part of the fermionic potential. Figures 5 and 6 show the $\text{Re}[L_F]$ - $\text{Im}[L_F]$ relation for three-flavor EPLMWO and Z_3 -EPLM, respectively. We set $\mu = 0.95M$, since the sign problem is severest in the vicinity of $\mu = 0.95M$ (or $1.05M$), as seen in the next section. Both the figures have qualitatively the same structure, but their physical meanings are much different. In Z_3 -EPLM, the confinement state $P_x = 0$ and the deconfinement states $P_x = 1, e^{\pm i2\pi/3}$ are degenerate on the left vertex where the sign problem is absent and $e^{-\text{Re}[L_{F,Z_3}]}$ is largest. Meanwhile, in EPLMWO only the state $P_x = 1$ is present on the left vertex. More generally, the states $P_x = b$ and $P_x = b e^{\pm i2\pi/3}$ ($b = -1/3 \sim 1$) are degenerate in Z_3 -EPLM, but not in EPLMWO. There is a tendency that, in both of EPLMWO and Z_3 -EPLM, the absolute value of $\text{Im}[L_F]$ becomes large, when the absolute value of $\text{Re}[L_F]$ is large. The absolute values of $\text{Re}[L_F]$ and $\text{Im}[L_F]$ themselves, however, are much smaller in Z_3 -EPLM than in EPLMWO. The latter property comes from the fact that the mass M present in L_{F,Z_3} is always multiplied by a factor of 3 and the absolute value $|L_{F,Z_3}|$ is more suppressed than $|L_F|$.

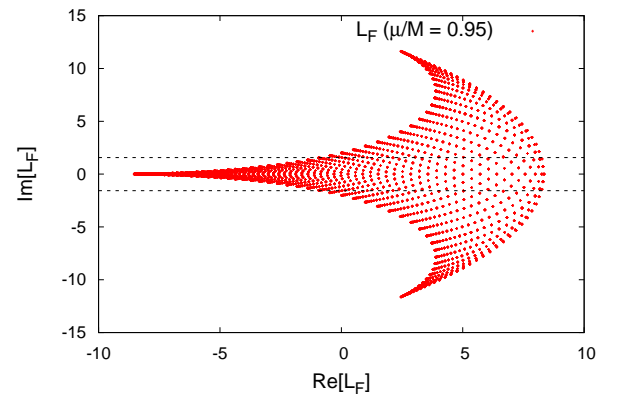


Fig. 5: The $\text{Re}[L_F]$ - $\text{Im}[L_F]$ relation in the 3 flavor EPLMWO. We set $M/T = 10$ and $\mu/M = 0.95$.

In Fig. 5 (Fig. 6), we see that the maximum value of the absolute value of $\text{Im}[L_F]$ ($\text{Im}[L_{F,Z_3}]$) is larger (smaller)

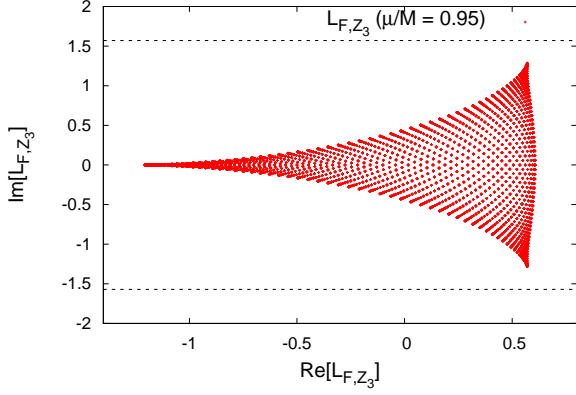


Fig. 6: The $\text{Re}[L_{F,Z_3}]$ - $\text{Im}[L_{F,Z_3}]$ relation in Z_3 -EPLM. We set $M/T = 10$ and $\mu/M = 0.95$.

than $\frac{\pi}{2}$ at $\mu/M = 0.95$. This means that, at $\mu/M = 0.95$, the sign of $\cos(\text{Im}[L_{F,Z_3}])$ is always positive in Z_3 -EPLM, while the sign of $\cos(\text{Im}[L_F])$ is not definite in EPLMWO. Hence, in Z_3 -EPLM with $N_s = 1$, there is no sign problem at $\mu/M = 0.95$ when $N_s = 1$. However, even in Z_3 -EPLM, the absolute value of $S_{F,I} = \sum_{\mathbf{x}} \text{Im}[L_{F,Z_3}(\mathbf{x})]$ can be large and $\cos(S_{F,Z_3,I})$ can have a negative sign when N_s increases. This causes the sign problem in Z_3 -EPLM with larger N_s , although it is milder than in EPLMWO.

C. Improved reweighting method

In order to improve PQRW, we assume that the realization probability of the configuration with S_R and S_I is well approximated by the probability distribution function proportional to $e^{-S_R} e^{-\alpha S_I^2}$, where α is an appropriate parameter that may depend on κ , μ and N_s . In fact, Ejiri studied the distribution of the phase of the quark determinant by using the Taylor expansion method and found that it can be well approximated by a Gaussian function [48]. Similar analysis was made with the strong coupling expansion method [49].

We consider the following approximation:

$$\begin{aligned} \langle O \rangle'' &= \frac{\int \mathcal{D}\varphi_r \mathcal{D}\varphi_g O(\varphi_{r,\mathbf{x}}, \varphi_{g,\mathbf{x}}) F''(\varphi_{r,\mathbf{x}}, \varphi_{g,\mathbf{x}})}{Z''}; \\ F''(\varphi_{r,\mathbf{x}}, \varphi_{g,\mathbf{x}}) &= e^{-S_0 - S_{F,R}} e^{-\alpha S_{F,I}^2}, \\ Z'' &= \int \mathcal{D}\varphi_r \mathcal{D}\varphi_g F''(\varphi_{r,\mathbf{x}}, \varphi_{g,\mathbf{x}}), \end{aligned} \quad (40)$$

In actual simulations, we treated α as a variable parameter and searched a best value for α .

As shown in the case of PQRW, the ratio $W'' = Z/Z''$ is

given by

$$\begin{aligned} W'' &= \frac{Z}{Z''} = \frac{\int \mathcal{D}\varphi_r \mathcal{D}\varphi_g \left[e^{-iS_{F,I}} e^{\alpha S_{F,I}^2} \right] F'(\varphi_{r,\mathbf{x}}, \varphi_{g,\mathbf{x}})}{Z''} \\ &= \langle e^{-iS_{F,I}} e^{\alpha S_{F,I}^2} \rangle'' = \left\langle \frac{F}{F''} \right\rangle''. \end{aligned} \quad (41)$$

Taking the partial average of two configurations $(\varphi_{r,\mathbf{x}}, \varphi_{g,\mathbf{x}})$ and $(\varphi'_{r,\mathbf{x}}, \varphi'_{g,\mathbf{x}})$ that satisfy $(\varphi'_{r,\mathbf{x}}, \varphi'_{g,\mathbf{x}}) = (-\varphi_{r,\mathbf{x}}, -\varphi_{g,\mathbf{x}})$, we obtain [34]

$$\begin{aligned} W'' &= \frac{\int \mathcal{D}\varphi_r \mathcal{D}\varphi_g \left[\cos(S_{F,I}) e^{\alpha S_{F,I}^2} \right] F''(\varphi_{r,\mathbf{x}}, \varphi_{g,\mathbf{x}})}{Z''} \\ &= \langle \cos(S_{F,I}) e^{\alpha S_{F,I}^2} \rangle'', \end{aligned} \quad (42)$$

since $S_{F,I}(\varphi'_{r,\mathbf{x}}, \varphi'_{g,\mathbf{x}}) = -S_{F,I}(\varphi_{r,\mathbf{x}}, \varphi_{g,\mathbf{x}})$. Unlike the case of PQRW, the condition $|W''| \leq 1$ is not ensured in this case. If F'' is a good approximate probability distribution function, $W'' \sim \tilde{W}'' \equiv \langle e^{\alpha S_I^2} \rangle'' \geq 1$ is expected instead of $W'' \sim 1$. Using the reweighting method, we can obtain the true expectation value $\langle O \rangle$ as

$$\begin{aligned} \langle O \rangle &= \frac{\int \mathcal{D}\varphi_r \mathcal{D}\varphi_g [O(\varphi_{r,\mathbf{x}}, \varphi_{g,\mathbf{x}})] F(\varphi_{r,\mathbf{x}}, \varphi_{g,\mathbf{x}})}{Z} \\ &= \frac{\int \mathcal{D}\varphi_r \mathcal{D}\varphi_g \left[O e^{-iS_{F,I}} e^{\alpha S_{F,I}^2} \right] F''}{Z''} \times \frac{Z''}{Z} \\ &= \frac{\langle O e^{-iS_{F,I}} e^{\alpha S_{F,I}^2} \rangle''}{W''}. \end{aligned} \quad (43)$$

This reweighting method is referred to as ‘‘improved phase quenched reweighting (IPQRW)’’ in this paper.

D. Observables

In numerical calculations, we consider the following quantities as observables. First, we consider the spatial average \bar{P} of $P_{\mathbf{x}}$: Namely,

$$\bar{P} = \frac{1}{V} \sum_{\mathbf{x}} P_{\mathbf{x}}. \quad (44)$$

We calculate the expectation value of $|\bar{P}|$, since this quantity defines random and ordered states in the system and plays a role of the expectation value of Polyakov-line in QCD.

Another quantity is the quark number density given by

$$n_q = \frac{1}{\beta V} \frac{\partial(\log Z)}{\partial \mu} = \frac{1}{V} \frac{\partial \log Z}{\partial \hat{\mu}}, \quad (45)$$

where $\hat{\mu} = \mu/T$. LQCD at finite μ has the problem on the early onset of quark number density [21] or the baryon Silver Blaze problem [22]. The quark number density n_q should be zero at $T = 0$ for $\mu < M_N/3$, where M_N is the nucleon mass. However, it becomes finite in LQCD calculations for $\mu > m_\pi/2$ when PQRW is used, where m_π is the pion mass. Therefore, n_q is also useful to check whether our simulations are reliable or not.

V. NUMERICAL RESULTS

In this section, we present numerical evaluations of the phase factor W' (or the factor W'') and the expectation values of $|\bar{P}|$ and n_q . Our simulations were made by using the standard Monte Carlo algorithm. We consider three cases of $N_s = 6, 8, 12$. We also set $M/T = 10$ in this section, unless otherwise mentioned.

A. Results at $\mu = 0$

First we discuss the case of $\mu = 0$, since LQCD simulations have no sign problem there. Hence, the reweighting procedure is not needed. In Fig. 7, the κ -dependence of $\langle |\bar{P}| \rangle$ is shown for Z_3 -EPLM. As κ becomes large, $\langle |\bar{P}| \rangle$ increases. There is a rapid change of $\langle |\bar{P}| \rangle$ at $\kappa \sim 0.13$. The change seems to show a first-order phase transition, but we postpone our conclusion on the order since N_s in our simulations is not large enough to determine the order of the transition.

Figure 8 shows a sample of scatter plots of P_x at $\mu = 0$ for the case of Z_3 -EPLM. Note that any configuration sum is not taken in Fig. 8. Even in one configuration, at $\kappa = 0$, P_x widely distributes in the complex plane and $P_x = 0$ is not always ensured. However, the spatial average \bar{P} almost vanishes due to the cancellation among variables P_x on different lattice sites. At large κ , an ordered configuration of P_x is favored, and $\bar{P}_x \approx 1, e^{\pm i2\pi/3}$ is realized.

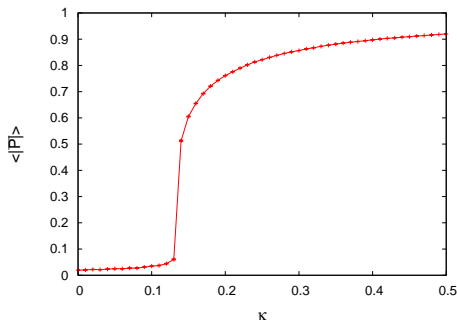


Fig. 7: The κ -dependence of expectation value $\langle |\bar{P}| \rangle$ at $\mu = 0$ in Z_3 -EPLM. We set $M/T = 10$, $\mu = 0$ and $N_s = 6$.

Similar result is obtained in EPLMWO, since the effect of the fermion action is small at $\mu = 0$ and Z_3 symmetry is almost preserved when M is large. If we use smaller mass $M = 5T$, the configurations of P_x at large κ are concentrated only in the vicinity of $P_x = 1$, since Z_3 symmetry is largely broken in EPLMWO with smaller M .

B. Phase quenched reweighting

EPLMWO and Z_3 -EPLM have the sign problem for finite μ . Hence, we use the reweighting method here.

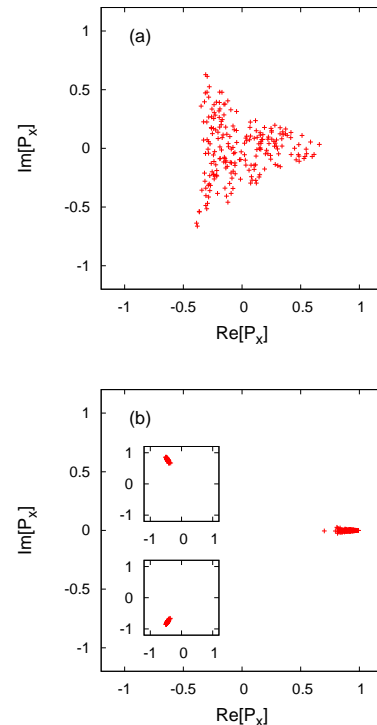


Fig. 8: The scatter plot of P_x at (a) $\kappa = 0$ and (b) $\kappa = 0.5$ in Z_3 -EPLM. We set $M/T = 10$, $\mu = 0$ and $N_s = 6$. Note that P_x in one configuration is plotted. In this configuration, P_x is concentrated in the vicinity of $P_x = 1$ when $\kappa = 0.5$. In the insets, configurations of P_x concentrated in the vicinity of $P_x = e^{i2\pi/3}$ and $P_x = e^{-i2\pi/3}$ are shown.

Figure 9 shows the phase factor for EPLMWO, where PQRW is used. Due to the P-H symmetry, in μ - κ plane, the result is almost symmetric with respect to the line $\mu = M$. It is seen that the sign problem is serious when $\mu/M = 0.5 \sim 1.5$ and $\kappa < 0.15$. For $\mu = M$, however, S_F is real and the phase factor is 1, as already mentioned in Sec. III A; note that these properties are not clearly seen in Fig. 9.

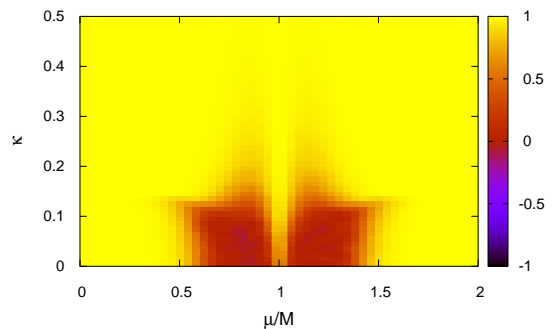


Fig. 9: The phase factor W' in EPLMWO, where PQRW is used. We set $N_s = 6$.

Figure 10 shows the phase factor for Z_3 -EPLM, where PQRW is used. The phase factor is small only in the region $\mu/M = 0.85 \sim 1.15$. (As in the case of EPLMWO, $W' = 1$ just on the line $\mu = M$.) For $\mu/M = 0.5 \sim 0.85$ ($1.15 \sim 1.5$) and $\kappa < 0.12$, the sign problem is considerably milder in Z_3 -EPLM than in EPLMWO. On the contrary, when $\mu/M = 0.85 \sim 1.15$ and $\kappa > 0.12$, the phase factor is somewhat smaller in Z_3 -EPLM than in EPLMWO. This may be originated in the fact that, as already seen in Sec. III D, L_{F,Z_3} is almost flat near $\mu = M$ and P_x can fluctuate considerably.

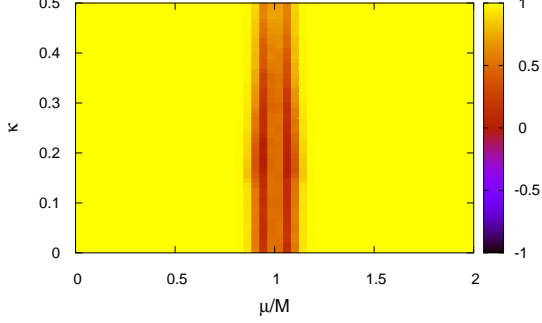


Fig. 10: The phase factor W' in Z_3 -EPLM, where PQRW is used. We set $N_s = 6$.

C. Improved phase quenched reweighting

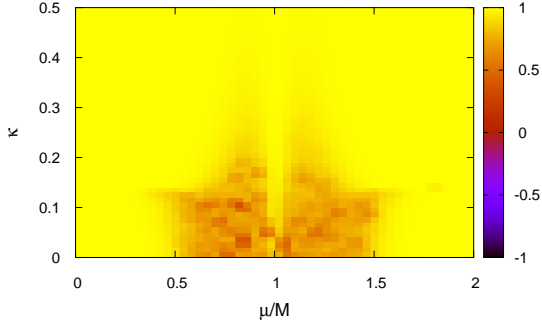


Fig. 11: The ratio W''/\tilde{W}'' in EPLMWO, where IPQRW is used. We set $\alpha = 3.5$ and $N_s = 6$.

Figure 11 shows W'' normalized by \tilde{W}'' for EPLMWO, where IPQRW is used. Note that the absolute value of the normalized W'' is not larger than the unnormalized one, since $\tilde{W}'' \geq 1$ is ensured. Comparing it with the W' obtained by PQRW, we can find that the absolute value of the normalized W'' becomes somewhat large. However, it is still considerably small when $\mu/M = 0.6 \sim 0.14$ and $\kappa < 0.12$ except for the line $\mu = M$.

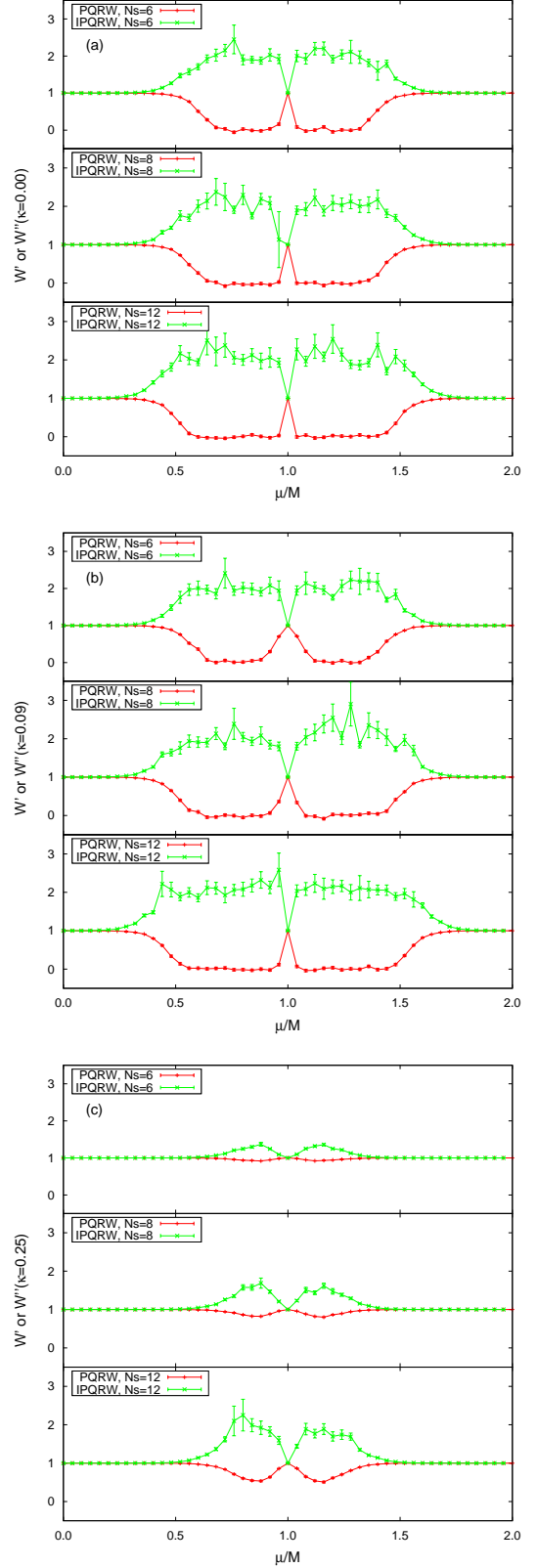


Fig. 12: The factors W' and W'' in EPLMWO at $M/T = 10$, where PQRW and IPQRW are used. We set $\alpha = 3.5$ in IPQRW. Note that W'' is not normalized in this figure. (a) $\kappa = 0$, (b) $\kappa = 0.09$, (c) $\kappa = 0.25$.

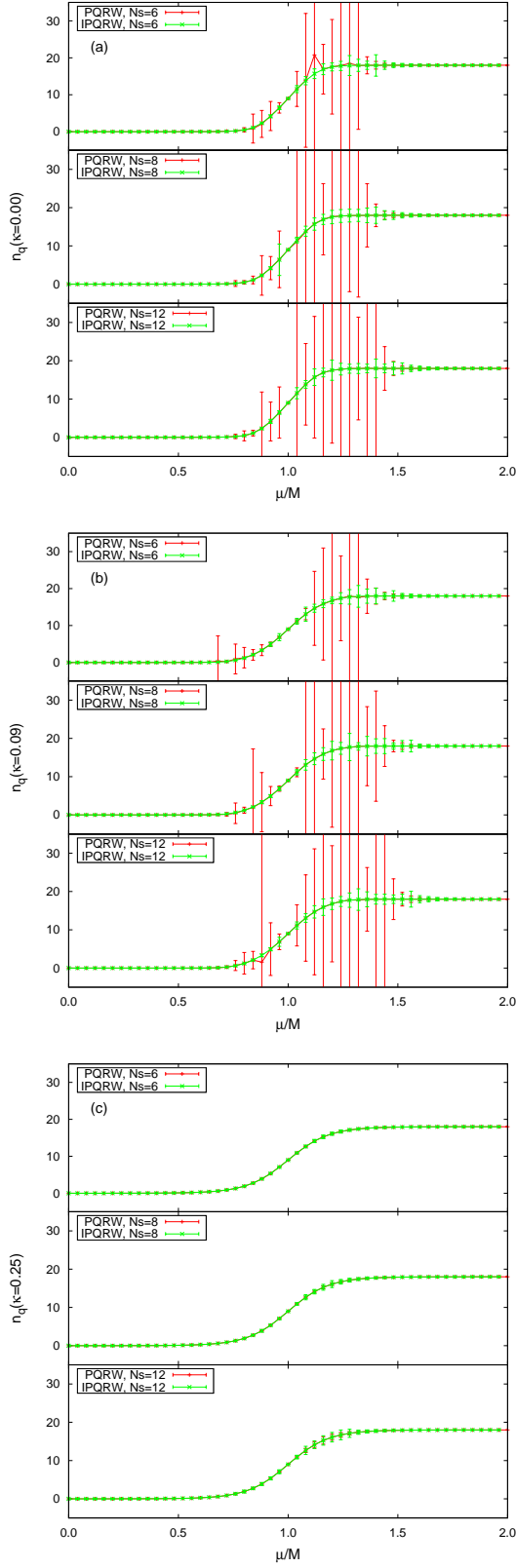


Fig. 13: The quark number density n_q in EPLMWO at $M/T = 10$, where PQRW and IPQRW are used. We set $\alpha = 3.5$ in IPQRW. (a) $\kappa = 0$, (b) $\kappa = 0.09$, (c) $\kappa = 0.25$.

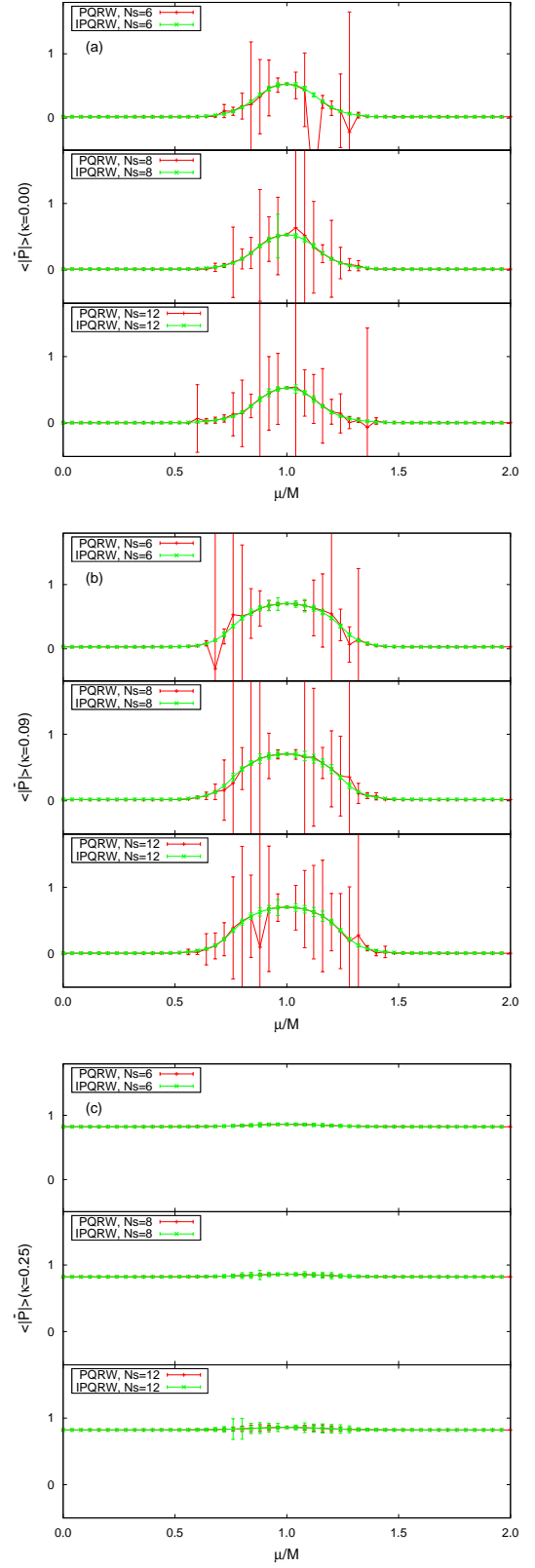


Fig. 14: The expectation value $\langle |\bar{P}| \rangle$ of the Polyakov line in EPLMWO at $\kappa = 0$, $M/T = 10$, where PQRW and IPQRW are used. We set $\alpha = 3.5$ in IPQRW. (a) $\kappa = 0$, (b) $\kappa = 0.09$, (c) $\kappa = 0.25$.

Figure 12 shows the μ dependence of W' and W'' for EPLMWO. In the region $\mu/M = 0.6 \sim 1.4$, the ratio W' in PQRW is close to zero except for the case of $\mu = M$, when $\kappa = 0$ and 0.09. In the same region, the ratio W'' in IPQRW lies between 1 and 2 but it fluctuates to some extent.

Figure 13 shows the μ dependence of n_q for EPLMWO. In the region $\mu/M = 0.6 \sim 1.4$ with $\kappa = 0$ and 0.09, due to the smallness of W' , the density n_q has a large error when PQRW is used, except for the case of $\mu = M$. When IPQRW is used, the error of n_q are small in the same region. In the figure, it is also seen that the N_s dependence is small when IPQRW is used.

Figure 14 shows the μ dependence of $\langle |\bar{P}| \rangle$ for EPLMWO. As in the case of n_q , in the region $\mu/M = 0.6 \sim 1.4$ with $\kappa = 0$ and 0.09, due to the smallness of W' , the expectation value $\langle |\bar{P}| \rangle$ has a large error when PQRW is used, except for the case of $\mu = M$. When IPQRW is used, the error of $\langle |\bar{P}| \rangle$ are small. Again, the N_s dependence is small, when IPQRW is used.

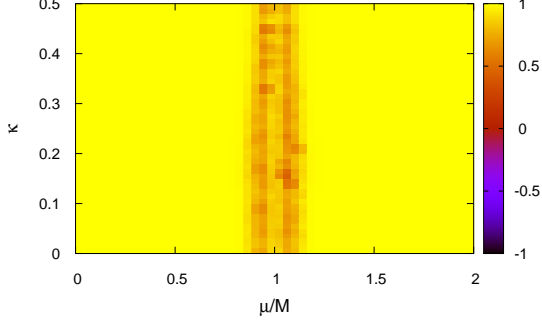


Fig. 15: The ratio W''/\tilde{W}'' in Z_3 -EPLM, where IPQRW is used. We set $\alpha = 3.5$ and $N_s = 6$.

Figure 15 shows the W'' normalized by \tilde{W}'' for Z_3 -EPLM, where IPQRW is used. The normalized W'' is close to 1 even in the vicinity of $\mu = M$. Even for small κ , the sign problem almost vanishes.

Figure 16 shows the μ dependence of W' and W'' for Z_3 -EPLM. For all the cases of κ , in the vicinities of $\mu/M = 0.95$ or 1.05, the ratio W' in PQRW is close to zero. In the same region, the ratio factor W'' in IPQRW is close to 2.

Figure 17 shows the μ dependence of n_q for Z_3 -EPLM. In the vicinity of $\mu/M = 0.95$ and also of $\mu/M = 1.05$, due to the smallness of W' , the density n_q has a large error except for the case of $\mu = M$ when PQRW is used. When IPQRW is used, the error of n_q is small. It is also seen that the N_s dependence is small, when IPQRW is used.

Figure 18 shows the μ dependence of $\langle |\bar{P}| \rangle$ for Z_3 -EPLM. For $\kappa = 0$ and 0.09, the mean value of $\langle |\bar{P}| \rangle$ almost vanishes for any μ . In the vicinity of $\mu/M = 0.95$ and also of $\mu/M = 1.05$, due to the smallness of W' , the expectation value $\langle |\bar{P}| \rangle$ has a large error when PQRW is used, except for the case with $\kappa = 0$ or 0.09 and $N_s = 6$, where the numerator of the last line in Eq. (39) vanishes almost completely. When IPQRW

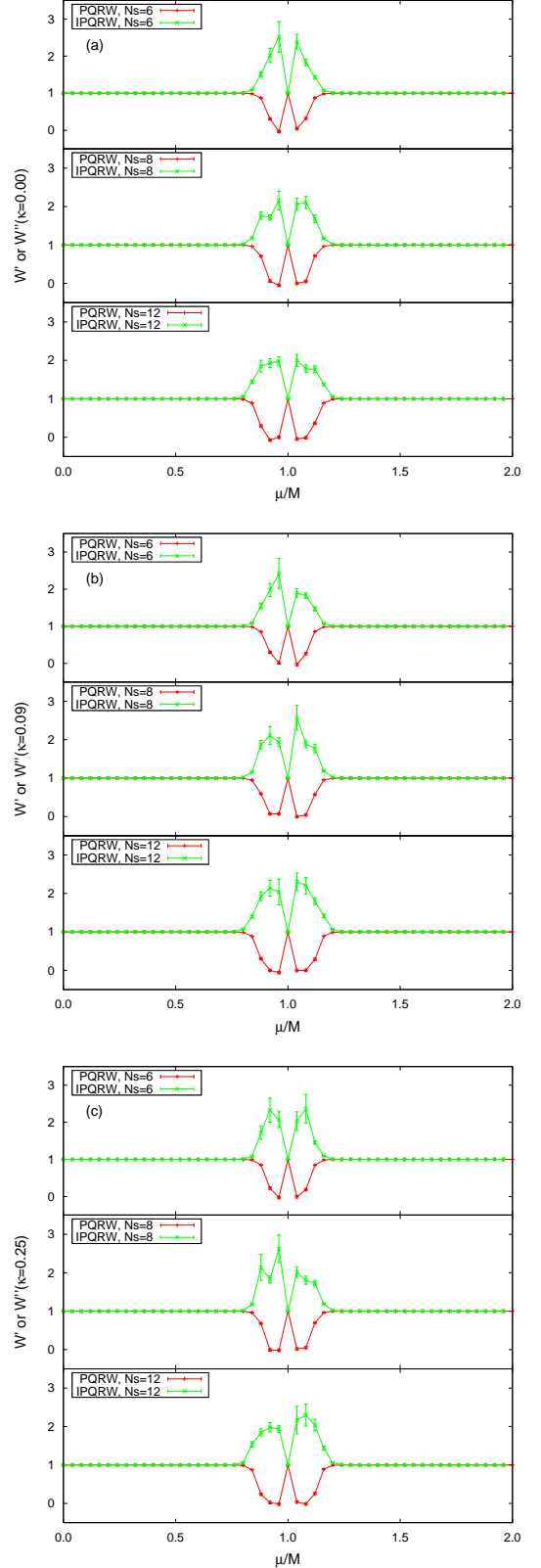


Fig. 16: The factors W' and W'' in Z_3 -EPLM at $\kappa = 0$, $M/T = 10$, where PQRW and IPQRW are used. We set $\alpha = 3.5$ in IPQRW. Note that W'' is not normalized in this figure. (a) $\kappa = 0$, (b) $\kappa = 0.09$, (c) $\kappa = 0.25$.

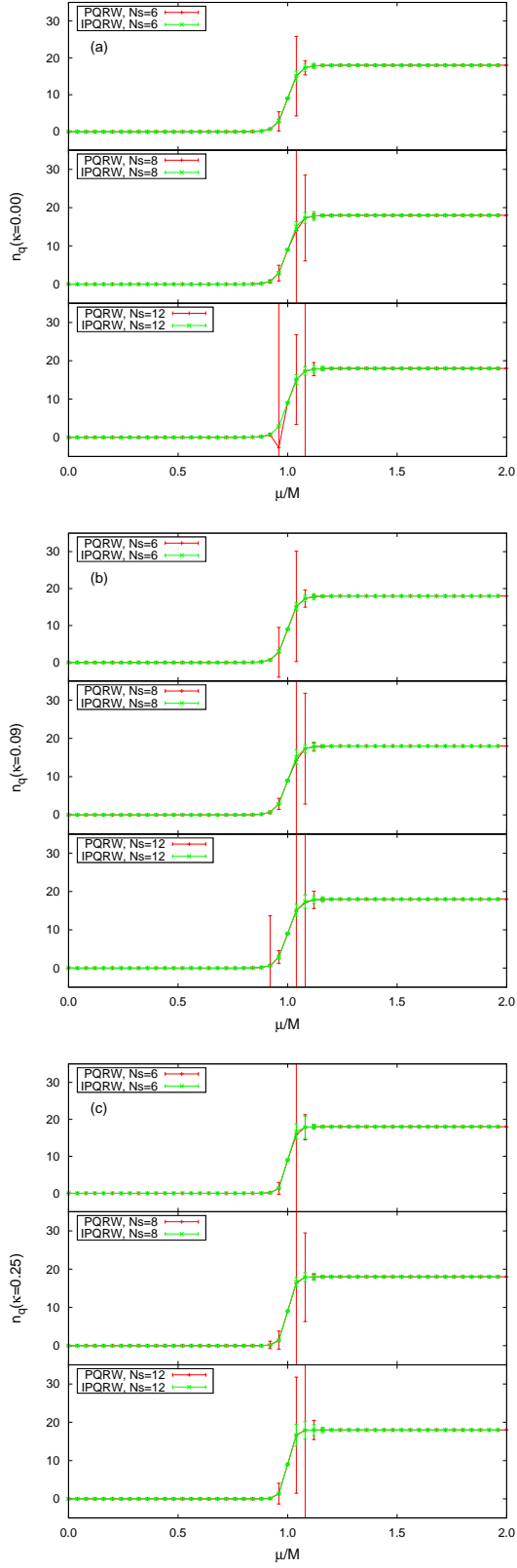


Fig. 17: The quark number density n_q in Z_3 -EPLM at $\kappa = 0$, $M/T = 10$, where PQRW and IPQRW are used. We set $\alpha = 3.5$ in IPQRW. (a) $\kappa = 0$, (b) $\kappa = 0.09$, (c) $\kappa = 0.25$.

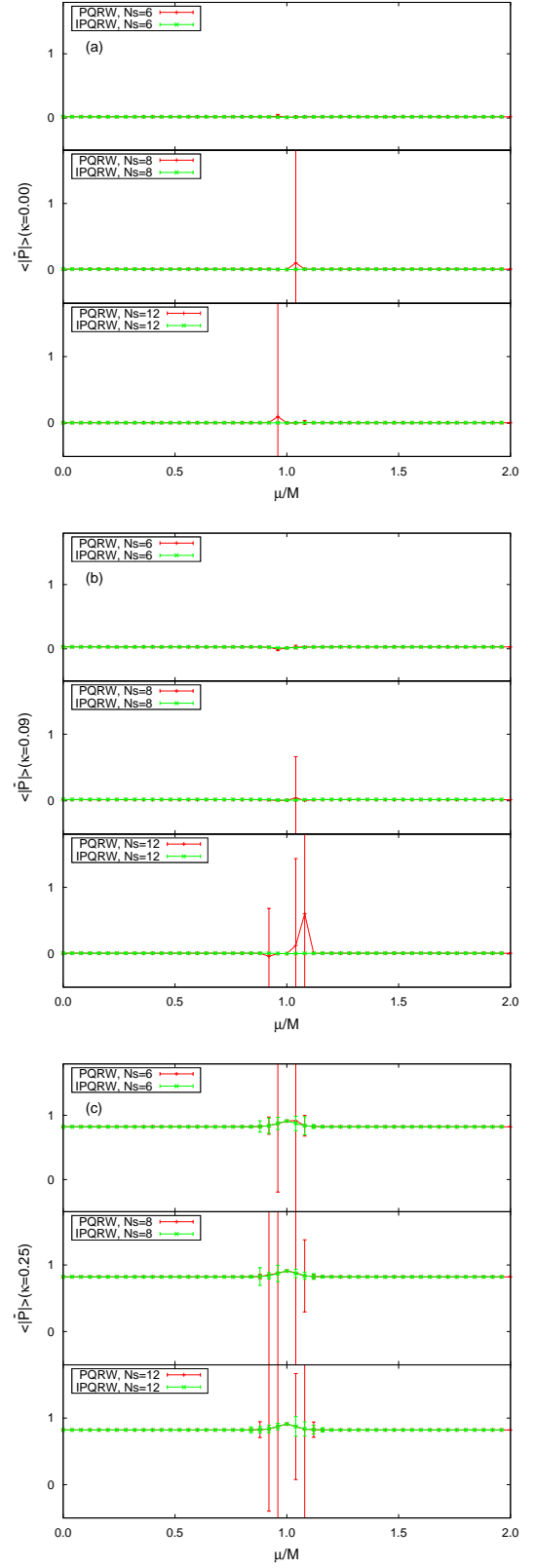


Fig. 18: The expectation value $\langle \bar{P} \rangle$ of the Polyakov-line in Z_3 -EPLM at $\kappa = 0$, $M/T = 10$, where PQRW and IPQRW are used. We set $\alpha = 3.5$ in IPQRW. (a) $\kappa = 0$, (b) $\kappa = 0.09$, (c) $\kappa = 0.25$.

is used, the error of $\langle |\bar{P}| \rangle$ are small. The N_s dependence is small in the figure when IPQRW is used.

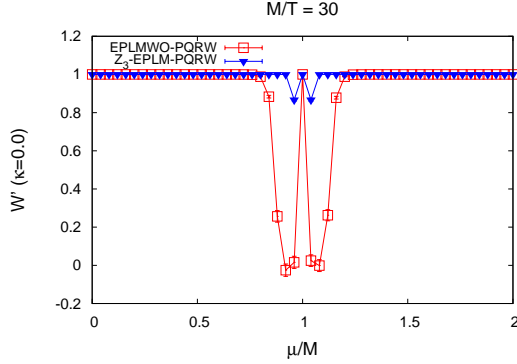


Fig. 19: The phase factors in EPLMWO and Z_3 -EPLM at $\kappa = 0$, $M/T = 30$, where PQRW is used.

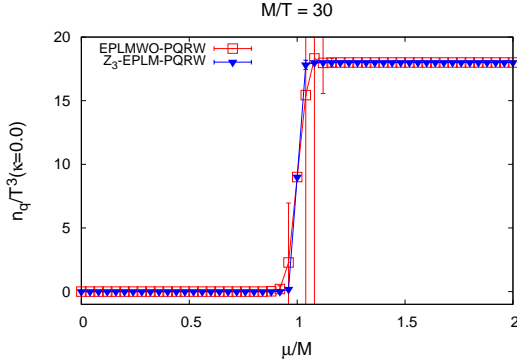


Fig. 20: The quark number density n_q in EPLMWO and Z_3 -EPLM at $\kappa = 0$, $M/T = 30$, where PQRW is used.

In the calculations mentioned above, the μ dependence of n_q at $\kappa = 0$ in Z_3 -EPLM is somewhat different from in EPLMWO. This result seems to be inconsistent with the expectation that Z_3 -EPLM tends to EPLMWO when $T \rightarrow 0$. However, in the calculations shown above, we have taken the case of $M/T = 10$. In the limit $T \rightarrow 0$, we should consider the limit $M/T \rightarrow \infty$ at the same time to put $\kappa = 0$. In Figs. 19 and 20, the μ dependences of the phase factor and n_q at $M/T = 30$ and $\kappa = 0$ are shown in both EPLMWO and Z_3 -EPLM, where PQRW is used. We see that the sign problem is very weak everywhere in Z_3 -EPLM while it is still strong at $\mu/M \sim 0.95$ in EPLMWO. The quark number density n_q in EPLMWO almost coincides with that in Z_3 -EPLM when the sign problem is weak in EPLMWO. This result indicates that Z_3 -EPLM tends to EPLMWO in the limit $T \rightarrow 0$. We also see that $n_q(\mu)$ is close to $18\theta(\mu - M)$ in Z_3 -EPLM, where $\theta(x)$ is a step function and 18 is the degree of freedom of quark. This suggests that the early onset of n_q does not appear at low T for the case of Z_3 -EPLM.

VI. SUMMARY

In summary, we have studied the sign problem in the Z_3 -symmetric effective Polyakov-line model (Z_3 -EPLM). In Z_3 -EPLM, the confinement state of $P_x = 0$ and the three deconfinement states based on Z_3 symmetry degenerate, when the pure gauge contribution is neglected. In other words, the pure gauge contribution is important to determine which state is more favorable. The Haar measure term favors the confinement state, while the gluonic kinetic term does the ordered deconfinement configurations.

In the confinement phase where the effect of gluonic kinetic term is small, the confinement state of $P_x = 0$ is favored but finite P_x is also realized to some extent as the fluctuations. However, the realized probability P_x is almost Z_3 -symmetric even in one configuration, and consequently, the spatial average $\bar{P} = \sum_x P_x$ almost vanishes. Meanwhile, in the deconfinement phase, the ordered configuration is favored and the spatial average \bar{P} is finite in one configuration. Due to Z_3 symmetry, the configuration average $\langle \bar{P} \rangle$ vanishes but $\langle |\bar{P}| \rangle$ does not.

Z_3 -EPLM has no sign problem, when either the confinement state or the three deconfinement states are realized. This is because P_x is real in both the confinement and deconfinement states. In fact, this happens in the case of Z_3 -symmetric 3 or 4 states Potts model [34].

In both the random confinement phase and the intermediate phase, however, P_x fluctuates considerably and has finite imaginary part. Hence, $\text{Im}[S_F]$ is finite for finite μ . This causes a sign problem. Nevertheless, due to the reality of the confinement and the deconfinement states mentioned above and the smallness of $\text{Im}[S_F]$, the sign problem is expected to be considerably milder in Z_3 -EPLM than in the ordinary EPLM with no Z_3 -symmetry. In fact, the results obtained by the phase quenched reweighting method show that the sign problem is considerably milder in Z_3 -EPLM than in the ordinary EPLM with no Z_3 -symmetry when κ is small.

We have also proposed the new reweighting method to include the contribution of the imaginary part of the fermion effective action into the approximate distribution function. The new method makes the sign problem somewhat milder. Particularly for in Z_3 -EPLM, the sign problem is very weak at small κ . It is also found that the results depend on N_s only weakly when the improved reweighting method is used.

Our results also indicate that the early onset of quark number density n_q does not appear in Z_3 -EPLM, when T is small. However, it may not be the case of Z_3 -QCD. The effective Polyakov-line model has the dynamics related to the Polyakov-line but is not expected to include the chiral dynamics in the calculation, since the quark mass is very large. In LQCD calculations, the pion-condensation-like phenomena appear as an artifact for finite μ , when the phase quenched reweighting is used. This artifact induces the problem on the early onset of quark number density [21] or the baryon-number Silver Blaze problem [22]. In the improved reweighting method proposed in this paper, contributions of the imaginary part of the fermion action are included into the approximated probability function to some extent. This improvement

may avoid the artifact mentioned above. It is very interesting to check whether this new method works well or not in LQCD simulations, particularly in lattice Z_3 -QCD.

Acknowledgments

The authors are thankful to Atsushi Nakamura, Hiroshi Yoneyama, Hiroshi Suzuki, Tatsuhiro Misumi, Etsuko Itou, Masahiro Ishii, Akihisa Miyahara, Shuichi Togawa, Yuhei Torigoe and K. Kashiwa for fruitful discussions. H. K. also

thanks Masahiro Imachi, Hajime Aoki, Motoi Tachibana and Takahiro Doi for useful discussions. J. S., H. K. and M. Y. are/were supported by Grant-in-Aid for Scientific Research (No.27-7804, No.17K05446 and No. 26400279, and No.26400278) from Japan Society for the Promotion of Science (JSPS). The numerical calculations were partially performed by using SX-ACE at Cybermedia Center and at RCNP, Osaka University.

-
- [1] Z. Fodor, and S. D. Katz, A new method to study lattice QCD at finite temperature and chemical potential, *Phys. Lett. B* **534**, 87 (2002).
- [2] C. R. Allton, S. Ejiri, S. J. Hands, O. Kaczmarek, F. Karsch, E. Laermann, Ch. Schmidt, and L. Scorzato, QCD thermal phase transition in the presence of a small chemical potential, *Phys. Rev. D* **66**, 074507 (2002).
- [3] S. Ejiri et al., Equation of state and heavy-quark free energy at finite temperature and density in two flavor lattice QCD with Wilson quark action, *Phys. Rev. D* **82**, 014508 (2010).
- [4] P. de Forcrand and O. Philipsen, The QCD phase diagram for small densities from imaginary chemical potential, *Nucl. Phys. B* **642**, 290 (2002).
- [5] M. D'Elia and M. P. Lombardo, Finite density QCD via an imaginary chemical potential, *Phys. Rev. D* **67**, 014505 (2003).
- [6] M. D'Elia and F. Sanfilippo, Order of the Roberge-Weiss endpoint (finite size transition) in QCD, *Phys. Rev. D* **80**, 111501 (2009).
- [7] P. de Forcrand and O. Philipsen, Constraining the QCD Phase Diagram by Tricritical Lines at Imaginary Chemical Potential, *Phys. Rev. Lett.* **105**, 152001 (2010).
- [8] K. Nagata and A. Nakamura, Imaginary chemical potential approach for the pseudocritical line in the QCD phase diagram with clover-improved Wilson fermions, *Phys. Rev. D* **83**, 114507 (2011).
- [9] J. Takahashi, K. Nagata, T. Saito, A. Nakamura, T. Sasaki, H. Kouno, and M. Yahiro, Color screening potential at finite density in two-flavor lattice QCD with Wilson fermions, *Phys. Rev. D* **88**, 114504 (2013); J. Takahashi, H. Kouno, and M. Yahiro, Quark number densities at imaginary chemical potential in $N_f = 2$ lattice QCD with Wilson fermions and its model analyses, *Phys. Rev. D* **91**, 014501 (2015).
- [10] G. Aarts, Can Stochastic Quantization Evade the Sign Problem? The Relativistic Bose Gas at Finite Chemical Potential, *Phys. Rev. Lett.* **102**, 131601 (2009).
- [11] G. Aarts and F. A. James, Complex Langevin dynamics in the SU(3) spin model at nonzero chemical potential revisited, *JHEP* **01**, 118 (2012).
- [12] G. Aarts, L. Bongiovanni, E. Seiler, D. Sexty, and I.-O. Stamatescu, Controlling complex Langevin dynamics at finite density, *Eur. Phys. J. A* **49**, 89 (2013).
- [13] D. Sexty, Simulating full QCD at nonzero density using the complex Langevin equation, *Phys. Lett. B* **729**, 108 (2014).
- [14] G. Aarts, F. Attanasio, B. Jager, E. Seiler, D. Sexty and I. O. Stamatescu, Exploring the phase diagram of QCD with complex Langevin simulations, *PoS LATTICE 2014*, 200 (2014) [arXiv:1411.2632 [hep-lat]].
- [15] J. Greensite, Comparison of complex Langevin and mean field methods applied to effective Polyakov line models, *Phys. Rev. D* **90**, 114507 (2014).
- [16] M. Cristoforetti et al., New approach to the sign problem in quantum field theories: High density QCD on a Lefschetz thimble, *Phys. Rev. D* **86**, 074506 (2012).
- [17] H. Fujii, D. Honda, M. Kato, Y. Kikukawa, S. Komatsu and T. Sano, Hybrid Monte Carlo on Lefschetz thimble – A study of the residual sign problem, *JHEP* **1310**, 147 (2013).
- [18] Y. Tanizaki, H. Nishimura, K. Kashiwa, Evading the sign problem in the mean-field approximation through Lefschetz-thimble path integral, *Phys. Rev. D* **91**, 101701 (2015).
- [19] Y. Tanizaki and M. Tachibana, Multi-flavor massless QED₂ at finite densities via Lefschetz thimbles, *JHEP* **1702**, 081(2016),
- [20] K. Langfeld and A. Wipf, Fermi-Einstein condensation in dense QCD-like theories, *Annals of Phys.* **327** (2012), 994.
- [21] I.M. Barbour, and A.J. Bell, Complex zeros of the partition function for lattice QCD, *Nucl. Phys. B* **372**, 385 (1992); I.M. Barbour, S.E. Morrison, E.G. Klepfish, J.B. Kogut, and M.-P. Lombardo, The critical points of strongly coupled lattice QCD at nonzero chemical potential, *Phys. Rev. D* **56**, 7063 (1997); I.M. Barbour, S.E. Morrison, E.G. Klepfish, J.B. Kogut, and M.-P. Lombardo, Results on finite density QCD, *Nucl. Phys. Proc. Suppl.* **60A**, 220 (1998); I. Barbour, S. Hands, J.B. Kogut, M.-P. Lombardo, and S. Morrison, Chiral symmetry restoration and realization of the Goldstone mechanism in the U(1) Gross-Neveu model at non-zero chemical potential, *Nucl. Phys. B* **557**, 327 (1999).
- [22] T.D. Cohen, Functional Integrals for QCD at nonzero Chemical Potential and Zero Density, *Phys. Rev. Lett.* **91**, 222001 (2003).
- [23] J. Condella, and C. DeTar, Potts flux tube model at nonzero chemical potential, *Phys. Rev. D* **61**, 074023 (2000).
- [24] Y.D. Mercado, H.G. Evertz and C.Gattringer, QCD Phase Diagram According to the Center Group, *Phys. Rev. Lett.* **106**, 222001 (2011); C. Gattringer, Flux representation of an effective Polyakov loop model for QCD thermodynamics, *Nucl. Phys. B* **850**, (2011), 242; Y.D. Mercado and C. Gattringer, Monte Carlo simulation of the SU(3) spin model with chemical potential in a flux representation, *Nucl. Phys. B* **862**, (2012), 737; Y.D. Mercado, H.G. Evertz and C. Gattringer, Worm algorithms for the 3-state Potts model with magnetic field and chemical potential, *Comput. Phys. Commun.*, **183**, (2012), 1920.
- [25] J. Bloch, F. Bruckmann and T. Wettig, Subset method for one-dimensional QCD, *JHEP* **10** (2013) 140; J. Bloch, F. Bruckmann and T. Wettig, Complex Langevin in low-dimensional QCD: the good and the not-so-good, *PoS(LATTICE 2013)* **194**, arXiv:1508.05252; J. Bloch and F. Bruckmann, Positivity of

- center subsets for QCD, Phys. Rev. D **93**, 014508 (2016).
- [26] A. M. Polyakov, Thermal properties of gauge fields and quark liberation, Phys. Lett. **72B**, 477 (1978).
- [27] A. Miyahara, Y. Torigoe, H. Kouno, and M. Yahiro, Equation of state and transition temperatures in the quark-hadron hybrid model, Phys. Rev. D **94**, 016003 (2016); A. Miyahara, M. Ishii, H. Kouno, and M. Yahiro, Crossover-model approach to QCD phase diagram, equation of state and susceptibilities in the $2+1$ and $2+1+1$ flavor systems, arXiv:1704.06432.
- [28] H. Kouno, Y. Sakai, T. Makiyama, K. Tokunaga, T. Sasaki, and M. Yahiro, Quark-gluon thermodynamics with the Z_{N_c} symmetry, J. Phys. G: Nucl. Part. Phys. **39**, 085010 (2012).
- [29] Y. Sakai, H. Kouno, T. Sasaki, and M. Yahiro, The quarkyonic phase and the Z_{N_c} symmetry, Phys. Lett. B **718**, 130 (2012).
- [30] H. Kouno, T. Misumi, K. Kashiwa, T. Makiyama, T. Sasaki, and M. Yahiro, Differences and similarities between fundamental and adjoint matters in $SU(N)$ gauge theories, Phys. Rev. D **88**, 016002 (2013).
- [31] H. Kouno, T. Makiyama, T. Sasaki, Y. Sakai, and M. Yahiro, Confinement and Z_3 symmetry in three-flavor QCD, J. Phys. G: Nucl. Part. Phys. **40**, 095003 (2013).
- [32] H. Kouno, K. Kashiwa, J. Takahashi, T. Misumi, and M. Yahiro, Understanding QCD at high density from a Z_3 -symmetric QCD-like theory, Phys. Rev. D **93**, 056009 (2016).
- [33] T. Iritani, E. Itou, T. Misumi, Lattice study on QCD-like theory with exact center symmetry, arXiv:1508.07132, to appear in JHEP; T. Misumi, T. Iritani, E. Itou, Finite-temperature phase transition of $N_f = 3$ QCD with exact center symmetry, presented at the 33rd International Symposium on Lattice Field Theory, Lattice2015, 14-18 July 2015, Kobe International Conference Center, Kobe, JAPAN, arXiv:1510.07227.
- [34] T. Hirakidai, H. Kouno, J. Takahashi, and M. Yahiro, Interplay between sign problem and Z_3 symmetry in three-dimensional Potts models, Phys. Rev. D **94**, 014011 (2016).
- [35] T.A. DeGrand, Phase structure of QCD at high temperature with massive quarks and finite quark density: A $Z(3)$ paradigm, Nucl. Phys. **B225**, 590 (1983).
- [36] F. Karsch and S. Stickan, The three-dimensional, three-state Potts model in an external field, Phys. Lett. B **488**, 319 (2000).
- [37] M. Alford, S. Chandrasekharan J. Cox and U.-J. Wiese, Solution of the complex action problem in the Potts model for dense QCD, Nucl. Phys. **B602**, 61 (2001).
- [38] T. Rindlisbacher, and P. de Forcrand, Two-Flavor Lattice QCD with a Finite Density of Heavy Quarks: Heavy-Dense Limit and "Particle-Hole" Symmetry, J. High Energy Phys. **02**, 1 (2016).
- [39] A. Roberge and N. Weiss, Gauge theories with imaginary chemical potential and the phases of QCD, Nucl. Phys. **B275**, 734 (1986).
- [40] A. Hasenfratz, and D. Toussaint, Canonical ensembles and nonzero density quantum chromodynamics, Nucl. Phys. **B371**, 539 (1992).
- [41] A. Cherman, T. Schäfer, and M. Ünsal, Chiral Lagrangian from Duality and Monopole Operators in Compactified QCD, Phys. Rev. Lett. **117**, 081601 (2016).
- [42] Y. Liu, E. Shuryak, and I. Zahed, Instanton-dyon liquid model. V. Twisted light quarks, Phys. Rev. D **94**, 105013 (2016).
- [43] P. N. Meisinger, and M. C. Ogilvie, Chiral symmetry restoration and Z_N symmetry, Phys. Lett. B **379**, 163 (1996).
- [44] A. Dumitru, and R. D. Pisarski, Two-point functions for $SU(3)$ Polyakov loops near T_c , Phys. Rev. D **66**, 096003 (2002); A. Dumitru, Y. Hatta, J. Lenaghan, K. Orginos, and R. D. Pisarski, Deconfining phase transition as a matrix model of renormalized Polyakov loops, Phys. Rev. D **70**, 034511 (2004); A. Dumitru, R. D. Pisarski, and D. Zschiesche, Dense quarks, and the fermion sign problem, in a $SU(N)$ matrix model, Phys. Rev. D **72**, 065008 (2005).
- [45] K. Fukushima, Chiral effective model with the Polyakov loop, Phys. Lett. B **591**, 277 (2004).
- [46] C. Ratti, M. A. Thaler, and W. Weise, Phases of QCD: Lattice thermodynamics and a field theoretical model, Phys. Rev. D **73**, 014019 (2006); C. Ratti, S. Rößner, M. A. Thaler, and W. Weise, Thermodynamics of the PNJL model, Eur. Phys. J. C **49**, 213 (2007).
- [47] E. Megias, E. Ruiz Arriola, and L. L. Salcedo, Polyakov loop in chiral quark models at finite temperature, Phys. Rev. D **74**, 065005 (2006).
- [48] S. Ejiri, Existence of the critical point in finite density lattice QCD, Phys. Rev. D **77**, 014508 (2008).
- [49] A. Ohnishi and T. Ichihara, Preweighting method in Monte-Carlo sampling with complex action—Strong-Coupling Lattice QCD with $1/g^2$ corrections, as an example—, arXiv:1512.08458 [hep-lat].